Non-Poissonian Ultrashort Nanoscale Electron Pulses

Sam Keramati, Will Brunner, T. J. Gay, and Herman Batelaan

Phys. Rev. Lett. **127**, 180602 — Published 27 October 2021

DOI: 10.1103/PhysRevLett.127.180602

Non-Poissonian ultrashort, nanoscale electron pulses

Sam Keramati[1,*], Will Brunner[1], T. J. Gay[1], Herman Batelaan[1,†]

[1]*Department of Physics and Astronomy, University of Nebraska-Lincoln, Lincoln, NE 68588, USA*

The statistical character of electron beams used in current technologies, as described by a stream of particles, is random in nature. Using coincidence measurements of femtosecond pulsed electron pairs, we report the observation of sub-Poissonian electron statistics that are non-random due to two-electron Coulomb interactions, and that exhibit an anti-bunching signal of 1 part in 4. This advancement is a fundamental step towards observing a strongly quantum degenerate electron beam needed for many applications, and in particular electron correlation spectroscopy.

Particle correlation spectroscopy, developed towards the end of the last century, is being used in an ever-lengthening list of applications. Photon correlations can be used, e.g., for sizing particles such as biological molecules and in aeronautical velocimetry [1]. In heavy-ion collisions, two-particle correlation measurements reveal the femtometer-size geometry of the ion source [2], while identical-atom correlation techniques demonstrate the quantum statistical nature of atomic isotope distributions [3]. The famous work of Hanbury Brown and Twiss (HBT) [4,5] and its elucidation by Glauber [6] led to this use of identical particle quantum correlations. A key underlying idea in all these experiments is that without particle correlation it becomes harder to resolve structural detail as the particles get closer together, while with particle correlations, proximity of the interacting particles makes such details easier to resolve. Examples of this include the resolution of stellar radii using light [7] and the femtometer sizing of nuclear structure using pions [2].

For electron sources, we have not yet seen the development of correlation spectroscopy, although the recent studies of Kiesel et al. [8] and Kuwahara et al. [9] show the way forward. In these experiments, a reduction in the number of coincidences at a pair of detectors was observed for free electrons emanating

from small sources. The nano- and micron-scale size of the sources ensured that electrons were close together in the direction transverse to the electron beam axis. Nonetheless, the continuous cold-field emission [8] or nanosecond pulsed photoemission [9] of electrons in these investigations made it unlikely that the electrons were close together in time, so that the (expectedly) small detected deviation from random statistical behavior was found not to exceed 1 part in 1000, limited by the finite detection-time resolution.

Introducing new classes of electron beams has led [10-12] and should continue to lead [13,14] to new applications. As non-random correlation signals are strongly dependent on electron-electron proximity, and thus on the source size and the pulse duration, we expect that correlation spectroscopy can be used as a complement to streak imaging [15, 16] in the accumulation mode. Additionally, just as "femtoscopy" using the HBT effect probes the femtometer scale for high-energy collisions [2], using pulsed, correlated electrons provides a novel route to exploring small-scale surface phenomena at ultrafast time scales.

Electron-electron correlation can be caused by Coulomb interaction and this has been studied in relation to the spatial resolution of electron lithography and scanning electron microscopy [17] and recently in relation to the temporal resolution of ultrafast electron diffraction [18]. Charged particle interactions are not only of interest with respect to the improvement of energy and spatial resolution, but can lead to self-organizing structures as observed in ion beams [19]. To our knowledge, no observation of a deviation from random, Poissonian statistics has been reported for electron beams.

A strong deviation from Poissonian statistics can herald quantum-optical effects [6,20,21]. The bosonic quantum nature of photon HBT-bunching, leading to super-Poissonian statistics, can be compared to the fermionic nature of electron HBT-like anti-bunching, leading to sub-Poissonian statistics. These experimental signatures of spin-statistical dual quantum effects can also be caused by classically describable causes. For light such a cause can be thermal intensity fluctuations [22], while for electrons the cause can be Coulomb repulsion. For the purpose of observing the quantum statistical regime for electron beams, it is thus necessary to distinguish Coulomb pressure from Pauli blockade. Indeed, even though the anti-bunching signal in earlier work [8] was attributed to quantum degeneracy, later analyses indicated that Coulomb pressure may explain the observation [23-26]. The very recent observation of electron anti-

bunching [9] is the next important step as it combines polarized electron sources in an electron microscope with coincidence detection. The claim in that work is that the electron polarization dependence of the anti-bunching observation is due to the HBT effect and not to polarization-dependent trajectories of the photoemitted electrons. The recent advent of sub-micron femtosecond laser driven electron sources of spin-polarized electrons [27] can further assist coincidence techniques to help unravel the classical and quantum contributions; unlike Pauli "forces", Coulomb forces are not spin dependent.

In the experiments reported here, we used a Ti:Sapphire femtosecond laser oscillator to photoemit ultrashort electron pulses from the apex of a tungsten nanotip (Fig. 1a). This ensured that the electrons in each pulse were close together both transversely and temporally. Such a source was introduced by Hommelhoff et al. [28] and exists today in several laboratories [29-32]. However, the non-random nature of the pulsed electrons, the key finding of this work, has not been demonstrated until now. The time-coincidence technique we have used to characterize the pulsed electron beam has made its non-statistical nature manifest; we observe departures from the expected Poissonian distribution of one part in four for the two-electron coincidence rate associated with a single pulse.

The output beam of the laser had a pulse duration of approximately 100 fs with 13.2 ns between laser pulses. An incident laser pulse can give rise to two-electron pulse emission. Their coincidence detection rate can be reduced by a repulsive Coulomb force between the electrons (Fig.1b) or by Pauli blockade of symmetric spin states (Fig.1c). Our estimated emission rate of 10^7 s^{-1} and a repetition rate of 10^8 s^{-1} imply that most laser pulses produce no electrons. In this case, the probability of producing a larger number of electrons per pulse is correspondingly smaller for a random distribution.

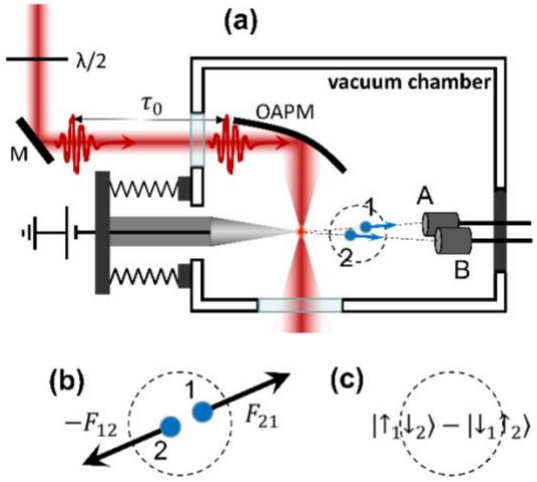

FIG. 1. Apparatus schematic. (a) Laser pulses (red) with a repetition time of τ_0, tightly focused on an electrochemically etched tungsten nanotip (gray cone) [33] using an off-axis parabolic mirror (OAPM), induced emission of, e.g., single electrons or electron pairs (blue circular dots). The electrons were detected by two independent detectors (A, B) and the time delay τ between their arrivals was measured in coincidence (see text). The coincidence detection rate characterizes the presence of electron-electron interactions and a deviation from random electron arrival times. The coincidence spectra were obtained using NIM electronics [34]. Two examples of possible interactions are: (b) a repulsive Coulomb force that may reduce the coincidence rate or (c) a Pauli blockade that only allows a singlet state to populate a symmetrical orbital which may reduce the coincidence rate.

For our detection probability, about one detected electron is produced for every 10^5 laser pulses, and a two-electron pulse occurs once for every ~10^7 laser pulses. Two electrons that arrive nearly simultaneously can be due to two electrons produced at the same time with nearly the same energy, but can also be due to two electrons produced at different times where the second electron has more energy

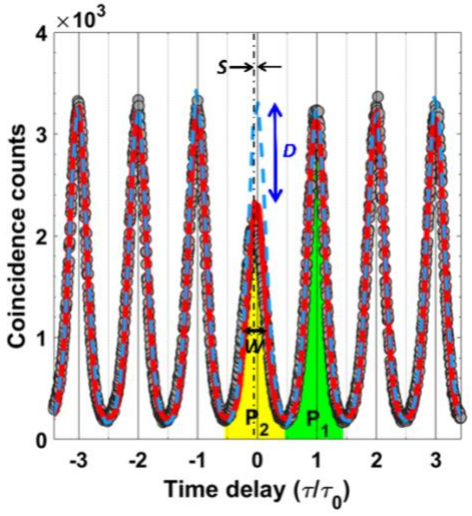

FIG. 2. Time delay coincidence spectrum. The experimental number of coincidence counts (circles) shows that the zero-time delay peak is smaller than its neighboring peaks. The zero-time delay peak contains two-electron pulses, while the neighboring peaks at integer multiples of the laser repetition time, $\tau_0 = 13.2\,ns$, contain single-electron pulses. A simulation of the experiment with a random number *n* of electrons per pulse in the absence of electron-electron interactions predicts identical heights for all peaks (dashed blue line). The random character in the simulation is given by a Poissonian distribution $P_n(\lambda)$, where $\lambda = r\tau_0$ and *r* is the emission rate. A simulation using two-electron pulses that includes mutual Coulomb interaction (red solid line) predicts a reduced central peak consistent with the experiment. The coincidence dip *D* is caused by the component of the mutual Coulomb force that is transverse to the electrons' motion. A small change in the width *W* and a small shift *S* of the zero-delay peak can also be attributed to the Coulomb force between the two electrons (see Supplemental Material).

and arrives at the same time as the first, lower-energy electron. This effect hampers experiments that are not time-resolved, but is significantly reduced for femtosecond pulsed sources when the pulses can be resolved in time.

The main experimental result is shown in Fig. 2, where the number of coincidences is shown as a function of the time delay between two detected electrons. The data acquisition time was 15 minutes. The

peak at zero-delay time is due almost exclusively to two electrons generated by the same laser pulse. The peak at $\tau = \tau_0$ is due to coincidence events where an electron generated by a laser pulse triggers the "start" detector, followed by another electron generated by the next laser pulse that triggers the stop detector. For the $\tau = 2\tau_0$ peak, the next laser pulse does not give rise to a stop trigger but the second-to-next laser pulse does, and so forth. An electronic time delay placed in the stop channel ensures that peaks with a negative time delay can also be recorded. The main observation of this work is that the zero-delay time peak is reduced compared to the surrounding peaks. We refer to this reduction as the "dip," and its presence is a clean signature that the statistical nature of the electron emission process is non-Poissonian [35]. The dip does not depend on the details of the detectors' efficiency or asymmetry.

To explain the presence of the dip in the zero-time delay peak, we performed a simulation with Coulomb interaction between the two electrons [36]. The simulation result (red solid line) agrees with the observed dip of Fig. 2 (circles). The transverse component of the mutual Coulomb force tends to push some electrons outside of the effective detection area (Fig. 3a and 3b), thereby lowering the coincidence counts in the zero-time delay peak. To find the height of the neighboring peaks, the mutual Coulomb interaction is turned off. Before continuing to a description of the simulation results, we present a summary of the method. In these calculations, pairs of electrons were considered and their motion was found by solving Newton's equations:

$$\begin{cases} m_e \, d^2\vec{r}_1 / dt^2 = \vec{F}_{tip,1} + \vec{F}_{1,2} + \vec{F}_{\mathrm{det},1} \\ m_e \, d^2\vec{r}_2 / dt^2 = \vec{F}_{tip,2} + \vec{F}_{2,1} + \vec{F}_{\mathrm{det},2} \end{cases}, \tag{1}$$

where the leading electron is labeled 1 and the trailing electron is labeled 2, m_e is the electron mass, $\left|\vec{F}_{1,2}\right| = \left|\vec{F}_{2,1}\right| = F_{qq}$ is the mutual electron interaction, and $\vec{F}_{\mathrm{det},1}$ ($\vec{F}_{\mathrm{det},2}$) is the Coulomb force exerted on electron *1* (*2*) by the detector entrance biased at V_f. These equations were solved numerically using the Runge-Kutta method. The nanotip apex is modeled as a hemisphere with radius R_{tip}. The electron's initial

positions are chosen randomly according to a uniform distribution on the hemisphere within a cone around the z-axis. The opening angle of the cone is chosen to correspond to the physical aperture in front of the detectors. The initial angle with respect to the normal of the hemisphere's surface follows a random cosine distribution. The azimuthal angle around the normal is distributed uniformly. These assumptions are motivated by the observation of 2-D images on a 2 cm diameter electron imaging system (Colutron BVS-1) at a distance of 5 cm from the nanotip showing a featureless electron pattern. The initial electron energy is uniformly distributed from 0 to 0.5 eV, and most of the acceleration to an approximate energy of 100 eV, due to the nanotip's electric field, occurs in the first few hundreds of nanometers. (Energy widths typically associated with multiphoton electron emission from tungsten do not significantly change the results of these simulations.) The accelerating force is indicated with F_{tip}. The second electron launches at a random time after the first electron within a time window Δt_{e} (10 fs for the result in Fig. 2).

By varying the strength of the Coulomb interaction in the simulation and inspecting the electron trajectories we find that the dip value *D* first increases as more electron pairs are pushed into the detectors (moving from region 1 to 2 in Fig. 3a and 3b), before it decreases when electrons are pushed outside the detection range (region 3 in Fig. 3a and 3b). The value of *D* increases with a decreasing time interval, Δt_e [36], between the electrons' emission times. For Gaussian shaped laser pulses, having intensity *I*(t) with a FWHM of 100 fs, the electron pulse duration is 50 fs for an I^4(t) (4-photon photoemission) process [37]. Such an estimate is valid for single-electron pulses. For the two-electron pulses recorded in the zero-delay peak, an intensity dependence $\propto I^8$ is expected. For Gaussian temporal envelopes, the standard deviation of τ is 30 fs, that is, about 68% of the electron pairs are emitted with a temporal separation of less than 30 fs. A simulated uniform pulse duration Δt_e of 10 fs yields a dip size that agrees with the experimental data. The tip radius R_{tip} was taken to be 25 nm. This is about half the value observed by SEM. The "lightning rod" effect [38] and the detector geometry, which selects electrons emitted in the forward direction, likely explains emission from a smaller size area and affects the detailed agreement between the expected and

simulated pulse duration. The main reported effect, that is, the reduction of the central peak, *D*, is robust and was observed for different tungsten nanotips.

We now show that Pauli blockade does not contribute to the dip. The Hanbury Brown-Twiss relative dip size due to Pauli blockade D_{HBT} (D_{HBT} = 0 for no dip; D_{HBT} = -1 corresponds to a complete dip) was studied in detail for 1D propagation [26]. For unpolarized electrons, straightforward generalization to 3D propagation yields the estimate

$$D_{\mathrm{HBT}} = -\frac{1}{2}\frac{\tau_{\mathrm{c}}}{\Delta t_{\mathrm{e}}}\frac{X_{\mathrm{c}}}{X_{\mathrm{tip}}}\frac{Y_{\mathrm{c}}}{Y_{\mathrm{tip}}}, \tag{2}$$

in which $\tau_{\mathrm{c}} \le \Delta t_{\mathrm{e}}$, $X_{\mathrm{c}} \le X_{\mathrm{tip}}$, and $Y_{\mathrm{c}} \le Y_{\mathrm{tip}}$ are the coherence time and lengths and $X_{\mathrm{tip}} \square Y_{\mathrm{tip}}$ are the physical sizes of the tip. The minimum energy-time uncertainty relation limits the coherence time to $\tau_{\mathrm{c}} = \hbar/2\Delta E = 0.66\ fs$ for $\Delta E = 0.5\,eV$; the coherence lengths are estimated from the position-momentum uncertainty relation as follows. The angular width of the distribution of the electrons that hit the detectors is $\gamma = \tan^{-1}\left(\frac{\Delta_{wx} + X_{\mathrm{det}}}{L}\right)$, where X_{det} is the distance between the centers of the front openings of the detectors, Δ_{wx} is the opening size of the detectors and *L* is the distance from the tip to the detectors [36].

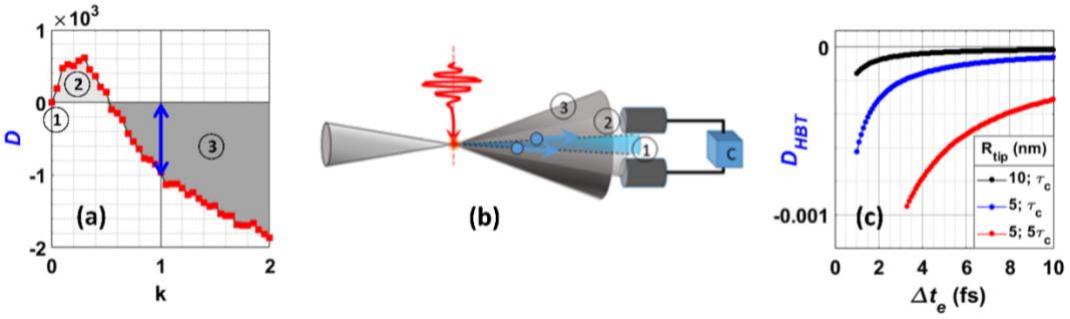

FIG. 3. Coulomb model. (a) The strength of the mutual Coulomb interaction k is varied in the model with k=1 corresponding to that which occurs in nature. In the absence of Coulomb interaction (region (1)), some forward propagating electron pairs miss the detectors. With increasing k, these electrons are pushed into the detectors increasing the number of coincidence counts *D* (region (2)). In region (3), the Coulomb interaction is strong enough to push electron pairs out of the detection

range so that *D* becomes negative. (b) The three trajectory regions described in (a) are illustrated schematically with three emission cones. (c) Pauli blockade due to quantum degeneracy is estimated to lead to a 0.01 – 0.1% reduction of the normalized coincidence count rate and thus cannot explain the observed 24% reduction. This conclusion is not changed when considering a significantly smaller tip apex radii, R_{tip}, a factor of two shorter pulse duration, and an extended coherence time of $5\tau_c$.

The transverse (*x*) component of the linear momentum uncertainty is $\Delta p_{\mathrm{x}} = p\gamma$, where $p = m_{\mathrm{e}}v$. The transverse coherence lengths are given by $X_{\mathrm{c}} = \hbar/2\Delta p_{\mathrm{x}}$ and $Y_{\mathrm{c}} = \hbar/2\Delta p_{\mathrm{y}}$, where $\Delta p_{\mathrm{y}} = p\tan^{-1}\left(\frac{\Delta_{wy}}{L}\right)$. The emission site lateral widths are estimated by $X_{\mathrm{tip}} = 2R_{\mathrm{tip}}\sin\gamma$, and $Y_{\mathrm{tip}} = X_{\mathrm{tip}}$. For these parameters the contribution of quantum degeneracy to anti-bunching is less than 1 part in 1000 (Fig. 3c).

An example of electron correlation spectroscopy is the use of the method described here to obtain the approximate duration of the electron pulse. To do this, the simulation model used to calculate the temporal spectrum (Fig. 2, red solid line) is simplified by calculating the impulse imparted to the electron along straight trajectories. This perturbative approach is motivated both by the result from the full simulation that trajectory deflection due to the mutual Coulomb forces is small, and the long computation times required for a full simulation. The result is that at large temporal separations the dip becomes negligible for all nanotip radii [39], substantiating the claim that an upper limit to the pulse duration can be estimated, and that for the experiment reported here the pulse is shorter than 10 fs.

Finally, we consider the pathway to observe electron beams with strong degeneracy. In our work, the transverse coherence can be increased by a diverging electron lens [8]. For a 100X magnifying lens, the detected transverse electron momentum is decreased and $X_{\mathrm{c}} = \hbar/2\Delta p_{\mathrm{x}}$ increased to reach full transverse coherence. In this case Eq. 2 becomes $D_{\mathrm{HBT}} = -\frac{1}{2}\frac{\tau_{\mathrm{c}}}{\Delta t}$, where Δt is either t_{pulse} or t_{detector}, depending on

whether the pulses are resolved in time or not. In earlier work [8,9,24] the longitudinal coherence was low which explains why the observed dips were limited to about 1 part in 1000, as the dip appears in the second order correlation function for unpolarized electrons as $g^{(2)} = 1 - t_c / 2\Delta t$. The addition of temporal resolution may thus lead to the observation of strong degeneracy. Note that the expression is the same as that for pulsed X-rays, for which $g^{(2)} = 1 - t_c / 2t_{pulse}$ [40]. This has been used as a method for determining X-ray pulse duration [41] and constitutes an example of photon correlation imaging. In our work the ratio of $t_{coherence}$ to t_{pulse} is about 10^{-1} and can be increased using an energy analyzer to reduce the energy spread of the detected electrons. An analyzing power of 1-100 meV corresponds to T_{coh} of ~100-1 fs. Analyzing powers reaching sub-10 meV have been realized [42], indicating that the observation of strong quantum degeneracy in an electron beam is, in principle, within reach [43]. The use of a femtosecond source could thus help reach the quantum degenerate regime. This was considered before [23, 44] but it led to a lower degeneracy [44] for the beam produced. Nevertheless, when the pulses are temporally resolved (Fig. 2a), the degree of degeneracy of the source is not necessarily a deciding factor if the goal is to observe a time-resolvable coincidence dip. Instead, the capability to compare the number of two-electron-events with single electron-events by post-selection becomes important.

In summary, we demonstrated that a tungsten nanotip electron source driven by femtosecond laser pulses exhibits a strong deviation from random Poissonian statistics. Because the pulses are time resolved, multi-electron pulses are distinguished from single-electron pulses even when the emission rate is low. Coulomb interactions explain our data and are sensitive to the tip apex radius and the electron pulse duration. As a result, this technique provides a method to characterize ultrashort electron pulse duration and photoemitting nanoscale structure size. The results also indicate that in HBT-type experiments with free electrons [8], the mutual Coulomb repulsion can contribute to the anti-bunching signal, and should not be neglected as it was in earlier work, as pointed out in refs. [23, 24, 25]. A larger source size and a longer pulse length can suppress the Coulomb interaction [9], while a diverging lens [8] and an energy analyzer can enhance the Pauli blockade in the observed signal. A laser-driven spin polarized source [9, 27] can

serve as a means to distinguish their relative contribution for femtosecond pulses [25, 26]. Femtosecond sources and time-resolved correlation techniques are expected to provide strong signals in the quantum regime. This provides access to new ideas in quantum statistics and the Pauli exclusion principle [45, 46, 47], leads to techniques that benefit from heralded single-electron on-demand sources such as quantum electron microscopy [14] and electron ghost imaging [48], may provide data for the theoretically unsolved problem of Coulomb interaction when electrons are mutually coherent, and helps develop entanglement-assisted [49] electron microscopy [50, 51] as well as ultrafast electron microscopy [52, 53].

S. Keramati and H. Batelaan acknowledge support for this work by the National Science Foundation (NSF) under the award number PHY-1912504, and the Nebraska Research Initiative. S. Keramati, W. Brunner and T. J. Gay acknowledge support by NSF under the award number PHY-1806771. The SEM images were taken at the NanoEngineering Research Core Facility (NERCF), which is partially funded by the Nebraska Research Initiative.

*sam.keramati@huskers.unl.edu

†hbatelaan@unl.edu

1. *Light Scattering and Photon Correlation Spectroscopy*, E.R.Pike and J.B. Abbiss, eds., NATO ASI Series 3. High Technology, Vol. 40 (Springer Science+Business Media, B.V., 1997)

2. Baym, G. The physics of Hanbury Brown–Twiss intensity interferometry: from stars to nuclear collisions. *Acta. Phys. Pol.* B **29**, 1839–1884 (1998).

3. Jeltes, T., et al. Comparison of the Hanbury Brown–Twiss effect for bosons and fermions, *Nature* **445**, 402–405 (2007).

4. Hanbury Brown, R. & Twiss, R.Q. A new type of interferometer for use in radio astronomy. *Philosophical Magazine* **45**, 663–682 (1954).

5. Hanbury Brown, R. & Twiss, R. Q. Correlation between Photons in two Coherent Beams of Light. *Nature* **177**, 27–29 (1956).

6. Glauber, R. J. *Quantum Theory of Optical Coherence. Selected Papers and Lectures* (Wiley-VCH, Weinheim, 2007).

7. Hanbury Brown, R. & Twiss, R.Q. A Test Of A New Type Of Stellar Interferometer On Sirius. *Nature* **178,** 1046–1048 (1956).

8. Kiesel, H., Renz, A. & Hasselbach, F. Observation of Hanbury Brown-Twiss anticorrelations for free electrons. *Nature* **418**, 392-394 (2002).

9. Kuwahara M., et al. Intensity Interference in a Coherent Spin-Polarized Electron Beam, *Phys. Rev. Lett.* **126**, 125501 (2021).

10. Zewail, A. H. Four-dimensional electron microscopy. *Science* **328**, 187-193 (2010).

11. Miller, R. J. D. Femtosecond crystallography with ultrabright electrons and X-rays: capturing chemistry in action. *Science* **343**, 1108-1116 (2014).

12. Arbouet, A., Caruso, G. M. & Houdellier, F. Ultrafast transmission electron microscopy: historical development, instrumentation, and application. *Advances in Imaging and Electron Physics* Vol. 207, pp 1-72. (Elsevier, Amsterdam, 2018).

13. Hassan, M. Th. Attomicroscopy: from femtosecond to attosecond electron microscopy. *J. Phys. B: At. Mol. Opt. Phys.* **51**, 032005 (2018).

14. Kruit, P. Designs for a quantum electron microscope. *Ultramicrosocopy* **164**, 31-45 (2016).

15. Liang, J., Zhu, L. & Wang, L.V. Single-shot real-time femtosecond imaging of temporal focusing. *Light Sci. Appl.* **7,** 42 (2018).

16. Gao, M. et al., Full characterization of RF compressed femtosecond electron pulses using ponderomotive scattering, *Optics Express* **20**, 12048-12058 (2012).

17. Jansen, G. H., Coulomb interactions in particle beams. *Nuclear Instruments and Methods in Physics Research* A **298**, 496-504 (1990).

18. Gordon, M., van der Geer, S. B., Maxson, J. and Kim, Y.-K., Point-to-point Coulomb effects in high brightness photoelectron beam lines for ultrafast electron diffraction. *Phys. Rev. Accel. Beams* **24**, 084202 (2021).

19. Murphy, D., Speirs, R.W., Sheludko, D.V., Putkunz, C.T., McCulloch, A.J., Sparkes, B.M. and Scholten R.E., Detailed observation of space–charge dynamics using ultracold ion bunches, *Nat. Comm.* 5:4489 (2014).

20. Hong, C. K., Ou, Z. Y. & Mandel, L. Measurement of subpicosecond time intervals between two photons by interference. *Phys. Rev. Lett.* **59** 2044–2046 (1987).

21. Jones, E., Becker, M., Luiten, J. & Batelaan, H. Laser control of electron matter waves, *Laser Photonics Rev.* **10**:2 214–229 (2016).

22. Loudon, R., Photon Bunching and Antibunching. *Phys. Bull.* **27** 21-23 (1976).

23. Baym, G. & Shen, K., *In Memory of Akira Tonomura*, Edited By: Kazuo Fujikawa and Yoshimasa A Ono. Hanbury Brown–Twiss Interferometry with Electrons: Coulomb vs. Quantum Statistics. 201-210 (World Scientific, Singapore, 2014).

24. Kodama, T., Osakabe, N. & Tonomura, A. Correlation in a coherent electron beam. *Phys. Rev. A* **83**, 063616 (2011).

25. Lougovski, P. & Batelaan, H. Quantum description and properties of electrons emitted from pulsed nanotip electron sources. *Phys. Rev. A.* **84**, 023417 (2011).

26. Keramati, S., Jones, E., Armstrong, J. & Batelaan, H. Partially coherent quantum degenerate electron matter waves. *Advances in Imaging and Electron Physics*. **213**, 3-26. (Elsevier, Amsterdam, 2020).

27. Brunkow, E., Jones, E. R., Batelaan, H. & Gay, T. J. Femtosecond-laser-induced spin-polarized electron emission from a GaAs tip, *Appl. Phys. Lett.* **114**, 073502 (2019).

28. Hommelhoff, P., Sortais, Y., Aghajani-Talesh, A. & Kasevich, M. A. Field Emission Tip as a Nanometer Source of Free Electron Femtosecond Pulses. *Phys. Rev. Lett.* **96**, 077401 (2006).

29. Ropers, C., Solli, D. R., Schulz, C. P., Lienau, C. & Elsaesser, T. Localized Multiphoton Emission of Femtosecond Electron Pulses from Metal Nanotips. *Phys. Rev. Lett.* **98**, 043907 (2007).

30. Barwick, B. et al. Laser-induced ultrafast electron emission from a field emission tip. *New J. Phys.* **9**, 142 (2007).

31. Yanagisawa, H., Optical Control of Field-Emission Sites by Femtosecond Laser Pulses. *Phys. Rev. Lett.* **103**, 257603 (2009).

32 . Vogelsang, J. Ultrafast Electron Emission from a Sharp Metal Nanotaper Driven by Adiabatic Nanofocusing of Surface Plasmons. *Nano Lett.* **15**, 4685 (2015).

33. See Supplemental Material at [URL will be inserted by publisher] for the nanotip manufacture procedure.

34. See Supplemental Material at [URL will be inserted by publisher] for coincidence circuitry.

35. See Supplemental Material at [URL will be inserted by publisher] for statistical analysis proofs.

36. See Supplemental Material at [URL will be inserted by publisher] for numerical simulation details.

37. Hilbert, S. A., Barwick, B., Fabrikant, M., Uiterwaal, C. J. G. J. & H. Batelaan. A high repetition rate time-of-flight electron energy analyzer. *Appl. Phys. Lett.* **91**, 173506 (2007).

38. Batelaan H. & Uiterwaal, C. J. G. J. Nature **446**, 500 (2007).

39. See Supplemental Material at [URL will be inserted by publisher] for temporal limits.

40. Classen, A., Ayyer, K., Chapman, H. N., Röhlsberger, R. & von Zanthier, J. Incoherent Diffractive Imaging via Intensity Correlations of Hard X Rays, *Phys. Rev. Lett.* **119**, 053401 (2017).

41. Yabashi, M., Tamasaku, K. & Ishikawa, T. Measurement of X-Ray Pulse Widths by Intensity Interferometry, *Phys. Rev. Lett.* **88**, 244801 (2002).

42. Allan, M. Threshold Phenomena in Electron-Molecule Scattering. *Phys. Scr.* **T110**, 161 (2004).

43. See Supplemental Material at [URL will be inserted by publisher] for a quantum degeneracy parameter map.

44. Kuwahara, M., The Boersch effect in a picosecond pulsed electron beam emitted from a semiconductor photocathode. *Appl. Phys. Lett.* **109**, 013108 (2016).

45. Silverman, M. P., On the feasibility of observing electron antibunching in a field-emission beam, *Phys. Lett.* A **120**, 442 (1987).

46. Kodama, T. Feasibility of observing two-electron interference, *Phys. Rev. A* **57**, 2781 (1998).

47. *Spin-Statistics connection and the commutation relations.*, Editors: Robert C. Hilborn, Gugliemo M. Tino (American Institute of Physics, Melville NY, 2000).

48. Li, S. et al. Electron Ghost Imaging, *Phys. Rev. Lett.* **121**, 114801 (2018).

49. Schattschneider, P. & Löffler, S. Entanglement and decoherence in electron microscopy.

Ultramicroscopy **190**, 39–44 (2018).

50. Okamoto, H. & Nagatani, Y. Entanglement-assisted electron microscopy based on a flux qubit. *Appl. Phys. Lett.* **104**, 062604 (2014).

51. Okamoto, H. Possible use of a cooper-pair box for low-dose electron microscopy. *Phys. Rev. A*, **85**, 043810 (2012).

52. Priebe, K. E. et al. Attosecond electron pulse trains and quantum state reconstruction in ultrafast transmission electron microscopy. *Nat. Photonics* **11**, 793-797 (2017).

53. Morimoto, Y. & Baum, P. Diffraction and microscopy with attosecond electron pulse trains. *Nat. Phys.* **14**, 252-256 (2018).